BIOMEDICAL ELECTRONIC DEVICES

15-nW Biopotential LPFs in 0.35-μm CMOS Using Subthreshold-Source-Follower Biquads with and without Gain Compensation

Tan-Tan Zhang, Pui-In Mak, Mang-I Vai, Peng-Un Mak, Man-Kay Law, Sio-Hang Pun, Feng Wan, and Rui P. Martins

FEATURES

Subthreshold-source-follower (SSF) Biquads
Improved noise and nonlinearity performance
Simple filter order extension by cascading
Low input-referred noise, < 36 μVrms
Silicon verified in standard 350nm bulk CMOS

DESCRIPTION

Extremely-low-power analog circuits continue to play a key role in wearable or implantable devices to achieve maximum system lifetime. However, existing biopotential acquisition systems still consume power in the range of tens to hundreds of μW.

This work focuses on the nW-class lowpass filter (LPF) in biopotential acquisition systems. The proposed SSF Biquad consists of four MOSFETs, two current sources and two floating capacitors, with no common-mode feedback (CMFB) required. A positive feedback loop exists to realize a complex pole and sharpen the stopband attenuation. At ultra-low frequency, the nonlinearity arising from the body-effect is pronounced, and the distortion is reduced with a higher DC level. When the frequency increases, the frequency-dependent effect becomes more pronounced as more AC current passes through the capacitive load.

The frequency-dependent distortion can be optimized by choosing a ~1:2 ratio for the source and drain capacitors. To solve the gain-loss due to the body effect, a gain-compensated (GC) scheme constructed by an extra cross-connected differential pair for extra gain is proposed. It can be demonstrated that the linearity is frequency dependent, and harmonic cancellation is possible by optimizing the bias current.

Two 4th-order 100-Hz-bandwidth LPFs using Butterworth approximation were designed. Replace this line with your descriptions. The first design is a non-GC NMOS-based SSF Biquad followed by a PMOS one (Fig. 1). The second design is a GC NMOS-based SSF Biquad followed by a PMOS one (Fig. 2). The measured and simulated gain performances of both LPFs are also shown.

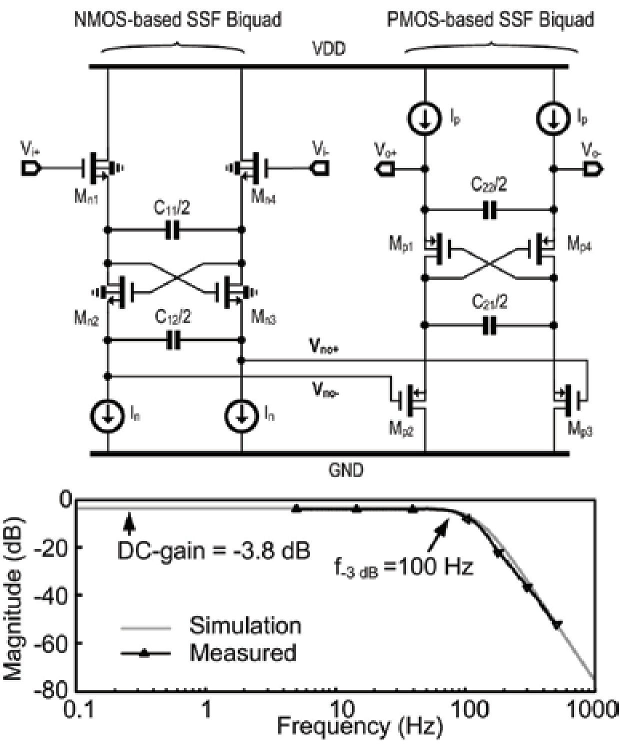

Fig. 1. Fabricated 4th-order non-GC LPF using SSF Biquads and measured gain performance.

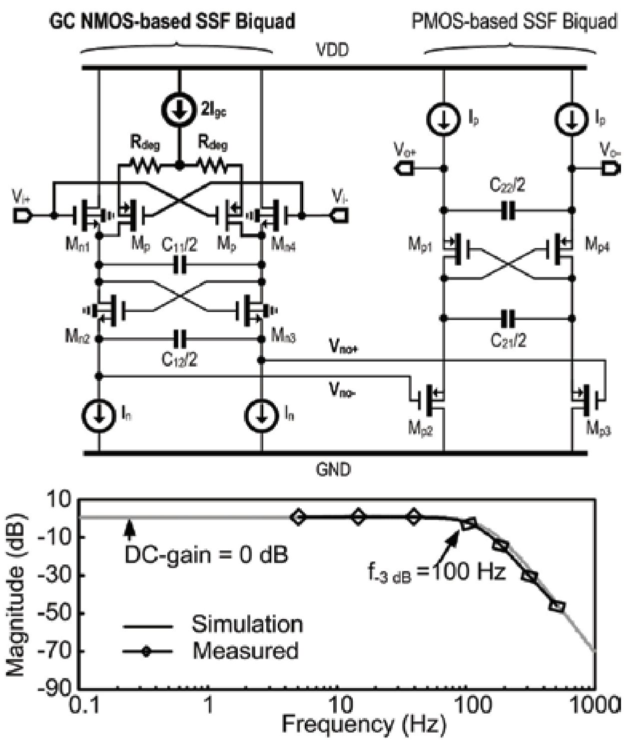

Fig. 2. Fabricated 4th-order GC LPF using SSF Biquads and measured gain performance.

Publication(s):

[1] T.-T. Zhang, P.-I. Mak, M.-I Vai, P.-U. Mak, M.-K. Law, S.-H. Pun, F. Wan, and R. P. Martins, "15-nW Biopotential LPFs in 0.35-μm CMOS Using Subthreshold-Source-Follower Biquads with and without Gain Compensation", IEEE Trans. Biomed. Circuits Syst., vol. 7, no. 5, pp. 690-702, Oct. 2013.

Sponsorship:

Macau Science and Technology Development Fund (FDCT), Research Committee of University of Macau

Energy Optimized Sub-threshold VLSI Logic Family with Unbalanced Pull-up/down Network and Inverse-Narrow-Width Techniques

Mingzhong Li, Chio-In Ieong, Man-Kay Law, Pui-In Mak, Mang-I Vai, Sio-Hang Pun, and Rui P. Martins

FEATURES

Low-voltage low-power sub-threshold logic cells
Unbalanced pull-up/down network with
Inverse-narrow-width technique
Transmission gate logic with logical effort optimization
High energy efficiency
Silicon verified in standard 0.18μm bulk CMOS

DESCRIPTION

Energy reduction achieved in sub-threshold operation is evidenced by the minimum energy point theory. However, the reduced overdrive voltage can dramatically worsen the device susceptibility in delay and noise margin due to process, voltage and temperature (PVT) variations, inevitably leads to sub-optimal performance in terms of power, delay and area, and even logic failure in the worst case.

This work presents a sub-threshold standard cell library targeting ultra-low-energy biomedical applications. In order to improve the energy efficiency, the unbalanced pull-up/down network, logical effort and inverse-narrow-width (INW) techniques are exploited. The unbalanced PU/PD network achieves a better energy efficiency as shown in Fig. 1(a), while the logical effort is utilized to qualitatively provide the delay spread estimate and distinguish dissimilar topologies of a particular logic for topology selection. The INW effect as shown in Fig. 1(b) is also exploited for circuit level optimization. Instead of using the smallest width per finger for both PMOS and NMOS transistors, analysis and silicon implementation of the INW effect using the power-delay-product (PDP) metric is initiated for optimal gate performance. An entity of 56 power-optimized sub-threshold logic cells using 0.3, 0.45 and 0.6V liberty files are implemented in standard 0.18μm CMOS (Fig. 1(c)). Measurement results from three 14-tap 8-bit FIR filters in Fig. 1(d) demonstrate substantial energy/cycle improvements.

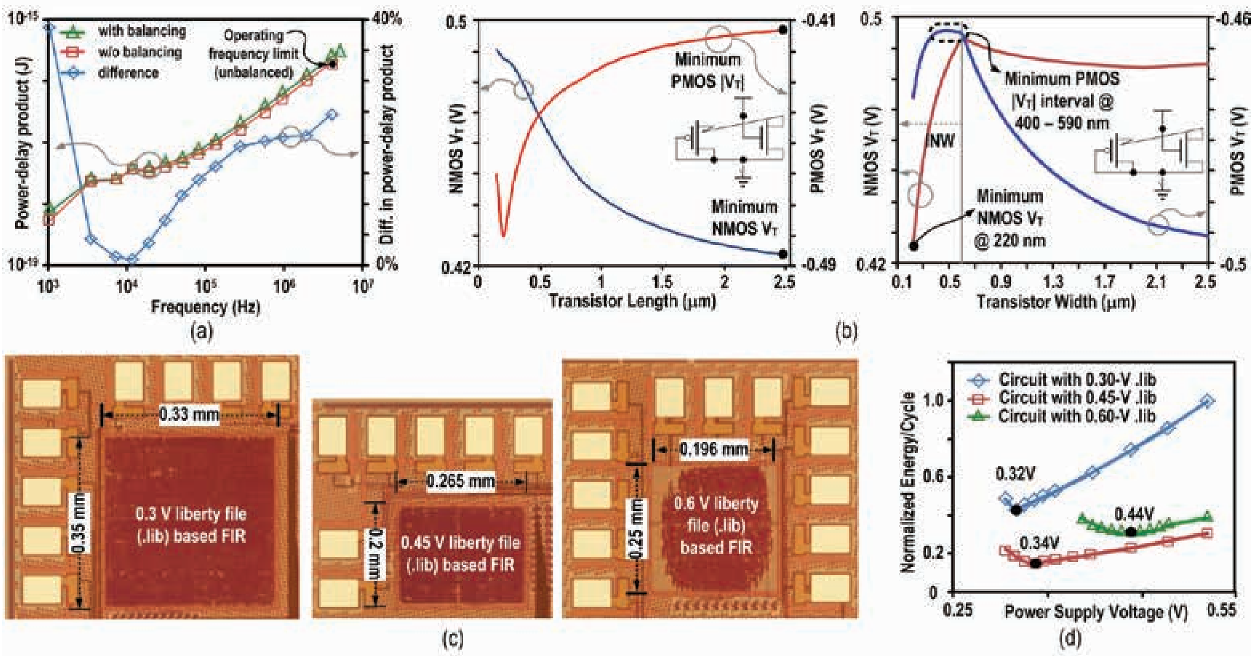

Fig. 1. (a) PDP of an inverter (FO4 loading) with balanced (P/N ratio = 5/1) and unbalanced (P/N ratio = 2/1) PU/PD network vs. operating frequency at 0.3 V. (b) NMOS/PMOS V_T vs. transistor length (RSC) (left) and transistor width (INW) (right) at V_{DD} = 0.3 V. (c) Die micrographs. (d) Normalized energy/cycle at different supplies.

Publication(s):

[1] M. Li, C.-I. Ieong, M.-K. Law, P.-I. Mak, M.-I Vai, S.-H. Pun, and R. P. Martins, "Energy Optimized Sub-threshold VLSI Logic Family with Unbalanced Pull-up/down Network and Inverse-Narrow-Width Techniques," IEEE Trans. Very Large Scale Integr. (VLSI) Syst., vol. 23, no. 12, pp. 3119-3123, Dec. 2015.

Sponsorship:

Macau Science and Technology Development Fund (FDCT), Research Committee of University of Macau

A Multi-Channel Power-Supply Modulated Micro-Stimulator With Energy Recycling

Paul Jung-Ho Lee, Man-Kay Law, Amine Bermak, and Jun Ohta

FEATURES

Multi-channel stimulation with energy recycling
Adiabatic forward buck/reverse boost operation
Digital pulse-skipping PWM quasi-PID controller supporting wide output power dynamics
High stimulation efficiency up to 1.23mA
Silicon verified in standard 180nm BCDLite CMOS

DESCRIPTION

We propose a multi-channel power-supply modulated micro-stimulator capable of energy recycling. By tracking the instantaneous electrode voltage, the thermal dissipation of the current drivers is reduced. Multi-channel stimulation is achieved through decoupling electrodes from the power supply while providing isolation for improved safety. The D-PS-PWM-QPID controller is proposed to deliver the required charge for regulating the modulated power supply under various stimulation scenarios without parameter tuning or external passive components.

Fig. 1 shows the proposed micro-stimulator employing a global switch-mode power supply (SMPS) that can be shared among all the electrode drivers for online dynamic voltage scaling (DVS) according to the electrode voltage. The SMPS modulates the voltage at the intermediate energy storage capacitor (C_{IESC}) through the forward buck/reverse boost operation to either feed charges into the electrodes in the anodic phase, or drain charges in the cathodic phase. C_{IESC} allows the proposed topology to decouple the individual electrode drivers from the power supply, facilitating adiabatic energy recycling over multiple electrodes with reduced control overhead.

The prototype chip is fabricated in standard 180nm BCDLite CMOS, with the chip photo and voltage waveforms as shown in Fig. 2. With supply voltage modulation and electrode charge recycling, our work achieves a power saving of up to 70%. By decoupling the power supply from the electrode using C_{IESC}, our proposed micro-stimulator enables highly scalable stimulation applications.

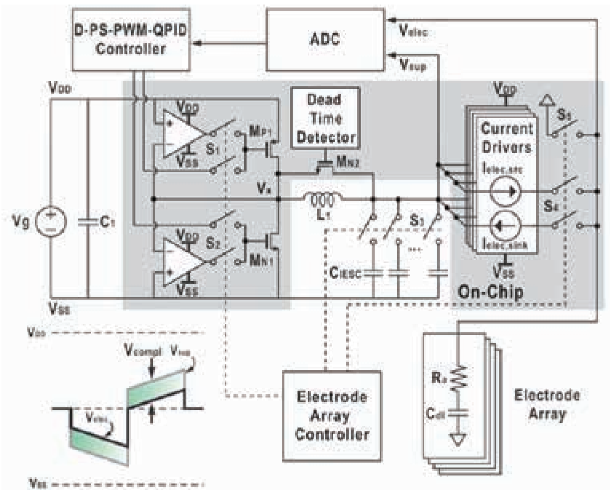

Fig. 1. Block diagram and of the proposed power-supply modulated micro-stimulator system and its output waveform during a biphasic stimulation cycle.

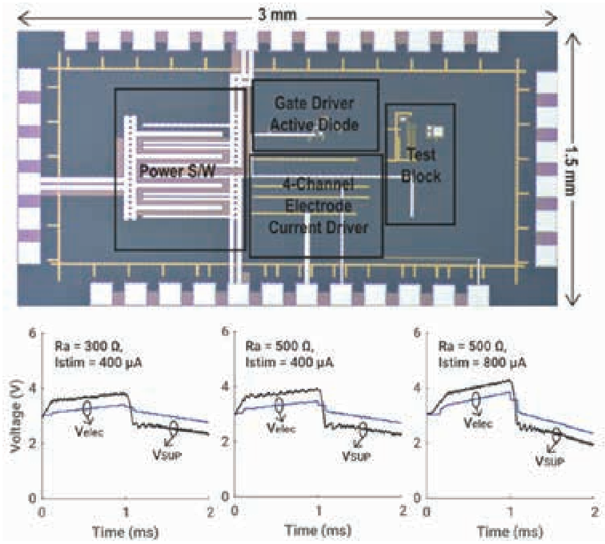

Fig. 2. Chip photo (top) and measured voltage waveforms during biphasic anodic first stimuli with different R_a and I_{stim}.

Publication(s):

[1] P. J.-H. Lee, M.-K. Law*, A. Bermak, and J. Ohta, "A Multi-Channel Power-Supply Modulated Micro-Stimulator With Energy Recycling," IEEE Des. Test, vol. 33, no. 4, pp. 61-73, Aug. 2016.

* Contributors with University of Macau

Sponsorship:

Macau Science and Technology Development Fund (FDCT), Research Committee of University of Macau, Hong Kong RGC Research Grant

A 0.45-V 147-to-375 nW ECG Compression Processor with Wavelet Shrinkage and Adaptive Temporal Decimation Architectures

Chio-In Ieong, Mingzhong Li, Man-Kay Law, Pui-In Mak, Mang-I Vai, and Rui P. Martins

FEATURES

Wavelet shrinkage
Adaptive temporal decimation
Modified Huffman and run-length wavelet source coding
Low power consumption, 147 – 375nW
Wide compression ratio, 2.89 – 26.91
Low %-RMS-distortion, 0 – 3.11%
Silicon verified in standard 180nm bulk CMOS

DESCRIPTION

This work investigates the design of a specialized ECG compression processor using wavelet shrinkage (WS), adaptive temporal decimation (ATD) and a combined modified Huffman and run-length wavelet source coding (MHRLC) architectures. Also, a set of energy-efficient low-voltage digital logic circuits optimized for low frequency operation are custom designed and employed.

Fig. 1 shows the three main modules of the proposed processor. WT type (mother wavelet) and architecture are firstly selected and designed, balancing the accuracy, CR and hardware efficiency. WS is optimized to enable global threshold estimation without PRD degradation. ATD is exploited to decimate the ECG signal adaptively by discriminating the QRS wave and P/T waves. The sparse wavelet coefficients are then compressed using the MHRLC optimized for the application.

The single-channel ECG data-compression processor is fabricated in a 1P6M 0.18-μm CMOS process, with an active area of 0.86 mm^2. With a 0.45-V supply and an external 360-Hz clock, this work provides higher CR and lower power consumption, as well as succeeds in providing a wide range of CR across lossless and lossy compression while preserving a low PRD. Overall, the WT and shrinkage architecture optimizations contribute to 46% power reduction to the overall design power, while ATD and near-threshold circuit causes a power reduction of 56.8% and 30.02%, respectively. The proposed power-efficient real-time ECG processor achieves low power consumption (375 – 147 nW at 0.45 V), wide range of CR (2.89 – 26.91) and low PRD (0 to 3.11%), making it suitable for long-term ECG monitoring.

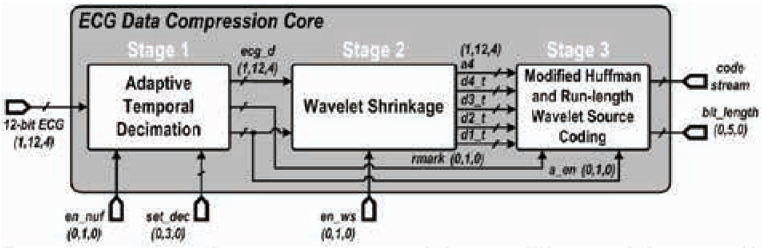

	This Work			Kim et al., Sym. VLSI'10	Chua et al., Tran. CE'11	Mamaghanian et al., EL'13
Verification Level	Experiment			Experiment	Simulation	Simulation
CMOS Tech. (nm)	180			180	65	180
VDD (V)	0.45			1.8	1	1
Operation Freq. (Hz)	360 (typical)			250-1k	24 M	100 M
Sampling Rate (Sa/s)	360 (typical)			250-1k	256	NA
BW (Bits)	12			16	10	NA
CR	**2.89**	**5.24**	**26.91**	8.4 or 2.1	2.38	2.43
PRD (%)	0	0.12	3.11	0.641	0	0
Power/Channel (μW)	**0.313**	**0.375**	**0.147**	6	56.6	36.4

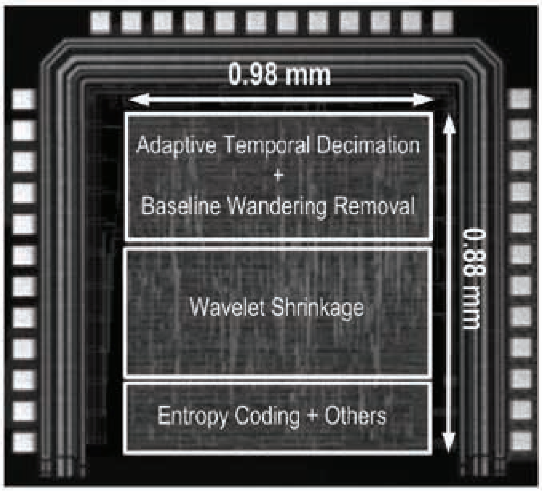

Fig. 1. Proposed ECG compression processor architecture (top left). Chip photograph (right). Performance comparison with state-of-the-art (bottom left).

Publication(s):

[1] C.-I. Ieong, M. Li, M.-K. Law, P.-I. Mak, M.-I Vai, and R. P. Martins, "A 0.45-V 147-to-375 nW Real-Time ECG Processor with Lossless-to-Lossy Data Compression for Wireless Healthcare Wearables," IEEE Trans. on Very Large Scale Integr. (VLSI) Syst., vol. 25, no. 4, pp. 1307-1319, Jan. 2017.

Sponsorship:

Macau Science and Technology Development Fund (FDCT), Research Committee of University of Macau

An Integrated Circuit for Simultaneous Extracellular Electrophysiology Recording and Optogenetic Neural Manipulation

Changhao Chen, Elizabeth A. McCullagh, Sio Hang Pun, Peng Un Mak, Mang I Vai, Pui In Mak, A. Klug, and Tim C. Lei

FEATURES

Low input capacitance of the amplifier, 9.7pF
Low input referred noise of the amplifier, 4.57μV_{rms}
High SNR, 6.6
Adequate LED/laser drive-current, max. 330 mA

DESCRIPTION

The ability to record and to control action potential firing in neuronal circuits is critical to understand how the brain functions. The objective of this study is to develop a monolithic integrated circuit (IC) to record action potentials and simultaneously control action potential firing using optogenetics.

A low-noise and high input impedance (or low input capacitance) neural recording amplifier is combined with a high current laser/light-emitting diode (LED) driver in a single IC.

The low input capacitance of the amplifier (9.7 pF) was achieved by adding a dedicated unity gain stage optimized for high impedance metal electrodes. The input referred noise of the amplifier is 4.57 μV_{rms}, which is lower than the estimated thermal noise of the metal electrode. Thus, the action potentials originating from a single neuron can be recorded with a signal-to-noise ratio of at least 6.6. The LED/laser current driver delivers a maximum current of 330 mA, which is adequate for optogenetic control. The functionality of the IC was tested with an anesthetized Mongolian gerbil and auditory stimulated action potentials were recorded from the inferior colliculus. Spontaneous firings of fifth (trigeminal) nerve fibers were also inhibited using the optogenetic protein Halorhodopsin. Moreover, a noise model of the system was derived to guide the design.

A single IC to measure and control action potentials using optogenetic proteins is realized so that more complicated behavioral neuroscience research and the translational neural disorder treatments become possible in the future.

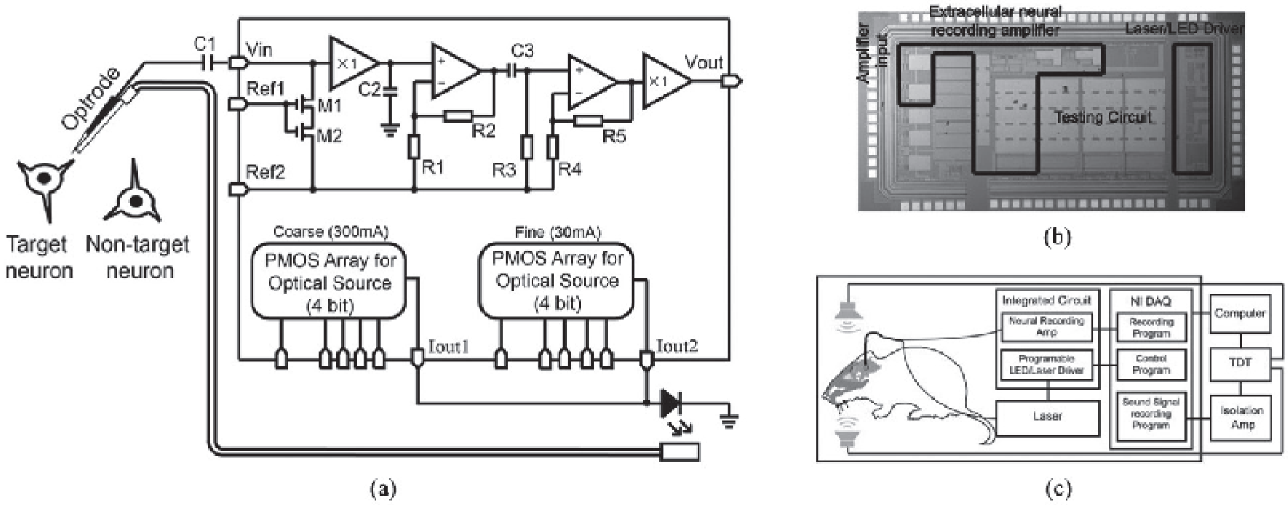

Fig. 1. (a) Schematic diagram of the IC integrating a high input impedance neural amplifier optimized of using a high impedance metal electrode for single neuron electrophysiology recording and two adjustable high current laser/LED drivers for optogenetic stimulation or inhibition; (b) Photograph of the fabricated IC with dimension of 2.9 mm × 1.6 mm. The actual neural amplifier and the laser/LED driver unit occupy about half of the space, with the rest of the space occupied by the additional testing circuits; (c) Experimental setup for simultaneous optogenetic inhibition and electrophysiological recordings from the brainstem of an anesthetized gerbil. The IC was connected to a data acquisition card (NI-DAQ) for signal digitization and laser power control. An isolation amplifier was used to isolate the neural amplifier from environmental noise. An audio signal processor (TDT) was used to generate a tonal signal to drive two speakers placed in the ears of the gerbil for auditory stimulation of the inferior colliculus.

Publication(s):

[1] C.H. Chen*, E. A. McCullagh, S.H. Pun*, P.U. Mak*, M.I Vai*, P.-I. Mak*, A. Klug, and T. C. Lei, "A Fully-Integrated Digital LDO with Coarse–Fine-Tuning and Burst-Mode Operation," IEEE Transactions on Biomedical Engineering, vol. 64, no. 3, pp. 557-568, Mar. 2017.

* Contributors with University of Macau

Sponsorship:

Macau Science and Technology Development Fund (FDCT), Research Committee of University of Macau, National Institutes of Health (NIH) NIDDK and Optogenetics and Neural Engineering Core at the University of Colorado NIH/NINDS.

Design of a Collapse-Mode CMUT With an Embossed Membrane for Improving Output Pressure

Yuanyu Yu, Sio Hang Pun, Peng Un Mak, Ching-Hsiang Cheng, Jiujiang Wang, Pui-In Mak, and Mang I Vai

FEATURES

An embossed membrane CMUT is proposed to improve output pressure

Developed a beam model to analyze the embossed membrane

The optimum position for the embossed pattern is predicted by the beam model

The output pressure is improved by 55.1% and 88.1% by Si_3N_4 and nickel pattern

DESCRIPTION

Capacitive micromachined ultrasonic transducers (CMUTs) have emerged as a competitive alternative to piezoelectric ltrasonic transducers, especially in medical ultrasound imaging and therapeutic ultrasound applications, which require high output pressure. However, as compared with piezoelectric ultrasonic transducers, the output pressure capability of CMUTs remains to be improved. In this paper, a novel structure is proposed by forming an embossed vibrating membrane on a CMUT cell operating in the collapse mode to increase the maximum output pressure. By using a beam model in undamped conditions and finite-element analysis simulations, the proposed embossed structure showed improvement on the maximum output pressure of the CMUT cell when the embossed pattern was placed on the estimated location of the peak deflection.

As compared with a uniform membrane CMUT cell worked in the collapse mode, the proposed CMUT cell can yield the maximum output pressure by 51.1% and 88.1% enhancement with a single embossed pattern made of Si_3N_4 and nickel, respectively. The maximum output pressures were improved by 34.9% (a single Si_3N_4 embossed pattern) and 46.7% (a single nickel embossed pattern) with the uniform membrane when the center frequencies of both original and embossed CMUT designs were similar.

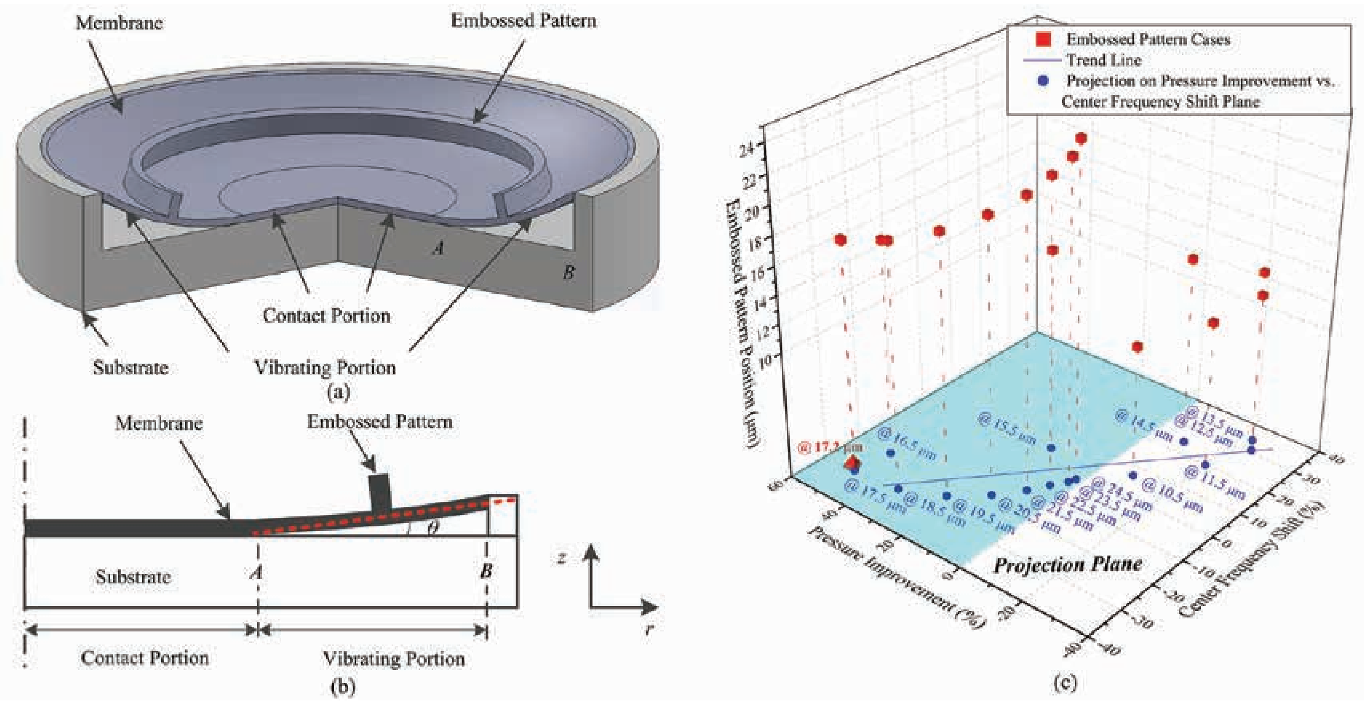

Fig. 1. (a) 3-D outlook view; (b) 2-D axisymmetric cross-sectional view of the proposed collapse-mode CMUT with an embossed membrane; (c) Relationship between pressure improvement and center frequency shift for various embossed positions.

Publication(s):

[1] Y.Y. Yu*, S.H. Pun*, P.U. Mak*, C.-H. Cheng, J.J. Wang*, P.-I. Mak*, and M.I Vai*, "Design of a Collapse-Mode CMUT With an Embossed Membrane for Improving Output Pressure," IEEE Transactions on Ultrasonics, Ferroelectrics, and Frequency Control, vol. 63, no. 6, pp. 854-863, Jun. 2016.

* Contributors with University of Macau

Sponsorship:

Macau Science and Technology Development Fund (FDCT), Research Committee of University of Macau

Output Pressure Enhancement of CMUTs by Using Multiple Helmholtz Resonance Apertures

Yuanyu Yu, Xue Wen Cao, Sio Hang Pun, Peng Un Mak and Mang I Vai

FEATURES

Helmholtz resonant is applied in CMUTs design
Arrangement of Helmholtz resonant apertures are investigated
The output pressure is improved by 32.1%

DESCRIPTION

Capacitive micromcachined ultrasonic transducer (CMUT) is a new generation ultrasonic transducer, which is an alternative to the dominating piezoelectric ultrasonic transducer. However, the output pressure of CMUT is still low that limits its application. To improve the output pressure is one pursuit in CMUT design.

In this paper, Helmholtz resonant structure is applied in an air-coupled CMUT to improve the output pressure. The spring soften effect to the CMUT resonant frequency is taken into account in calculating the Helmholtz resonance apertures. 3-D finite element method (FEA) models are constructed to evaluate the performance of this design. Single and multiple Helmholtz resonance apertures are investigated and compared with a conventional CMUT. It is found that the output pressure can be improved by 32.1% with four Helmholtz resonance apertures placed symmetrically in the membrane.

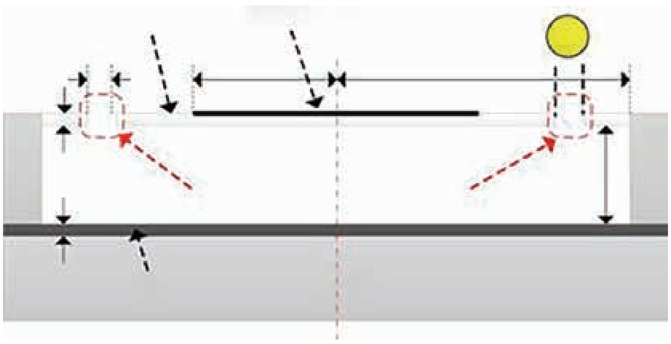

Fig. 1. Cross-section view of CMUT cell with Helmholtz resonance apertures (red dash line indicates central axis of CMUT cell (not in scale)).

Fig. 2. (a) 3D FEA model of CMUT cell and air domain: CMUT cell and air domain; (b) details of CMUT cell. All meshes except PML were smaller than 1/6 of wavelength of operating frequency; (c) Average output pressure over membrane: comparison between CMUTs with Helmholtz resonance apertures and conventional CMUT.

Publication(s):

[1] Y.Y. Yu, X.W. Cao, S.H. Pun, P.U. Mak and M.I Vai, "Output Pressure Enhancement of CMUTs by Using Multiple Helmholtz Resonance Apertures," Electronics Letters, vol. 51, no. 18, pp. 1390-1392, Sep. 2015.

Sponsorship:

Macau Science and Technology Development Fund (FDCT), Research Committee of University of Macau

Improved Analytical Modeling of Membrane Large Deflection With Lateral Force for the Underwater CMUT Based on Von Kármán Equations

Jiujiang Wang, Sio Hang Pun, Peng Un Mak, Ching-Hsiang Cheng, Yuanyu Yu, Pui-In Mak, and Mang I Vai

FEATURES

Low error in predicting displacement profile of conventional mode CMUT, <1%

Low error in predicting displacement profile of collapse mode CMUT, <4.7%

DESCRIPTION

This paper is to develop analytical models for the underwater capacitive micromachined ultrasonic transducer (CMUT) to understand its large deflection effect from the water pressure. To accurately model the displacement profile of the CMUT under the water pressure, Von Kármán equations and the perturbation method are employed to calculate the membrane deformation from a uniform pressure. The equations for an annular-ring plate model are first applied to calculate the displacement profile of the uniform CMUT membrane. The lateral force due to the membrane elongation is considered in the proposed model, which is used to calculate the displacement profiles for both conventional and collapse mode CMUTs under different external pressures.

When compared with finite-element method results, the proposed model can predict the displacement profiles of the conventional-mode CMUT under water pressure ranging from 0.8 to 4 MPa with an error of <1%. It can also estimate CMUT membrane that operates in collapse mode with an error in the deflection profile for <4.7% from 5 to 14 MPa. In addition, it is worth to mention that the proposed model can cover the small deflection scenarios but with relatively larger error under collapse mode.

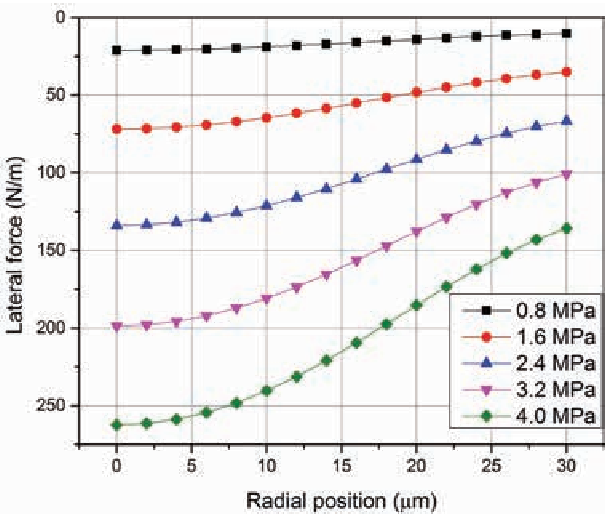

Fig. 1. Modeling results of lateral force for the large deflection membrane in conventional mode.

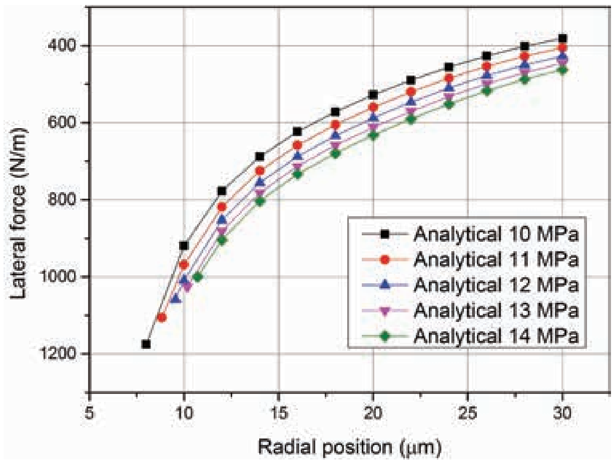

Fig. 2. Modeling results of the lateral force for the large deflection membranes in collapse mode.

Publication(s):

[1] J.J. Wang*, S.H. Pun*, P.U. Mak*, C.-H. Cheng, Y.YYu*, P.-I. Mak* and M.I Vai*, "Improved Analytical Modeling of Membrane Large Deflection With Lateral Force for the Underwater CMUT Based on Von Kármán Equations," IEEE Sensors Journal, vol. 16, no. 17, pp. 6633-6640, Sep. 2016.

* Contributors with University of Macau

Sponsorship:

Macau Science and Technology Development Fund (FDCT), Research Committee of University of Macau

Alpha neurofeedback training improves SSVEP-based BCI performance

Feng Wan, Janir Nuno da Cruz, Wenya Nan, Chi Man Wong, Mang I Vai, and Agostinho Rosa

FEATURES

Higher SSVEP signal SNR, 16.5% improved compared to the non-NFT control group

Higher BCI classification accuracy, 20.3% improved compared to the non-NFT control group

DESCRIPTION

Steady-state visual evoked potential (SSVEP)-based brain-computer interfaces (BCIs) can provide relatively easy, reliable and high speed communication. However, the performance is still not satisfactory, especially in some users who are not able to generate strong enough SSVEP signals. This work aims to strengthen a user's SSVEP by alpha down-regulating neurofeedback training (NFT) and consequently improve the performance of the user in using SSVEP-based BCIs.

An experiment with two steps was designed and conducted. The first step was to investigate the relationship between the resting alpha activity and the SSVEP-based BCI performance, in order to determine the training parameter for the NFT. Then in the second step, half of the subjects with 'low' performance (i.e. BCI classification accuracy <80%) were randomly assigned to a NFT group to perform a real-time NFT, and the rest half to a non-NFT control group for comparison.

The first step revealed a significant negative correlation between the BCI performance and the individual alpha band (IAB) amplitudes in the eyes-open resting condition in a total of 33 subjects. In the second step, it was found that during the IAB down-regulating NFT, on average the subjects were able to successfully decrease their IAB amplitude over training sessions. More importantly, the NFT group showed an average increase of 16.5% in the SSVEP signal SNR (signal-to-noise ratio) and an average increase of 20.3% in the BCI classification accuracy, which was significant compared to the non-NFT control group.

These findings indicate that the alpha down-regulating NFT can be used to improve the SSVEP signal quality and the subjects' performance in using SSVEP-based BCIs. It could be helpful to the SSVEP related studies and would contribute to more effective SSVEP-based BCI applications.

Group	Test	SSVEP SNR	Classification accuracy (%)
NFT	Test_1 (before NFT)	2.262 ± 0.685	65.4 ± 7.2
	Test_2 (after NFT)	2.635 ± 0.763	78.7 ± 6.3
Control	Test_1	2.431 ± 0.674	63.4 ± 14.7
	Test_2	2.378 ± 0.702	63.3 ± 14.6

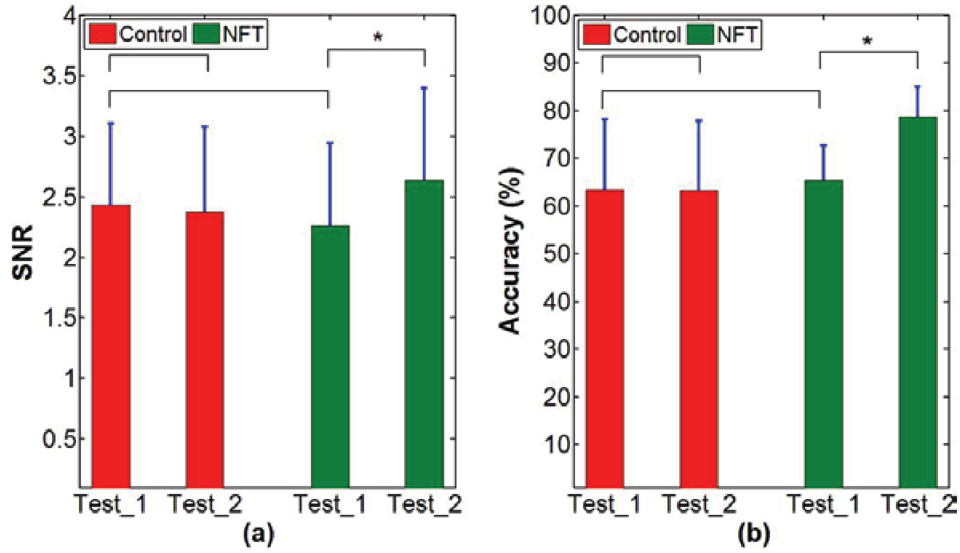

Fig. 1. Comparisons of the SSVEP-based BCI performance in the NFT and the control groups in terms of (a) the SSVEP SNR, and (b) the BCI classification accuracy. (Error bar indicates the SD, * represents the significant difference, p < 0.05).

Publication(s):

[1] F. Wan*, J. Nuno da Cruz*, W. Nan*, C.M. Wong*, M.I Vai* and A. Rosa, "Alpha neurofeedback training improves SSVEP-based BCI performance," Journal of Neural Engineering, vol. 13, no. 3, May 2016.

* Contributors with University of Macau

Sponsorship:

Macau Science and Technology Development Fund (FDCT), Research Committee of University of Macau

Effects of Human Limb Gestures on Galvanic Coupling Intra-body Communication for Advanced Healthcare System

Xi Mei Chen, Sio Hang Pun, Jian Feng Zhao, Peng Un Mak, Bo Dong Liang, and Mang I. Vai

FEATURES

Revealed the dynamic behavior of galvanic coupling IBC channel

Provided suggestions for practical IBC system design

DESCRIPTION

Intra-Body Communication (IBC), which utilizes the human body as the transmission medium to transmit signal, is a potential communication technique for the physiological data transfer among the sensors of remote healthcare monitoring system, in which the doctors are permitted to remotely access the healthcare data without interrupt to the patients' daily activities.

This work investigates the effects of human limb gestures including various joint angles, hand gripping force and loading on galvanic coupling IBC channel. The experiment results show that channel gain is significantly influenced by the joint angle (i.e. gain variation 1.09–11.70 dB, $p < 0.014$). The extension, as well as the appearance of joint in IBC channel increases the channel attenuation while the other gestures and muscle fatigue have negligible effect (gain variation <0.77 dB, $p > 0.793$) on IBC channel. Moreover, the change of joint angle on human limb IBC channel causes significant variation in bit error rate (BER) performance.

The results reveal the dynamic behavior of galvanic coupling IBC channel, and provide suggestions for practical IBC system design.

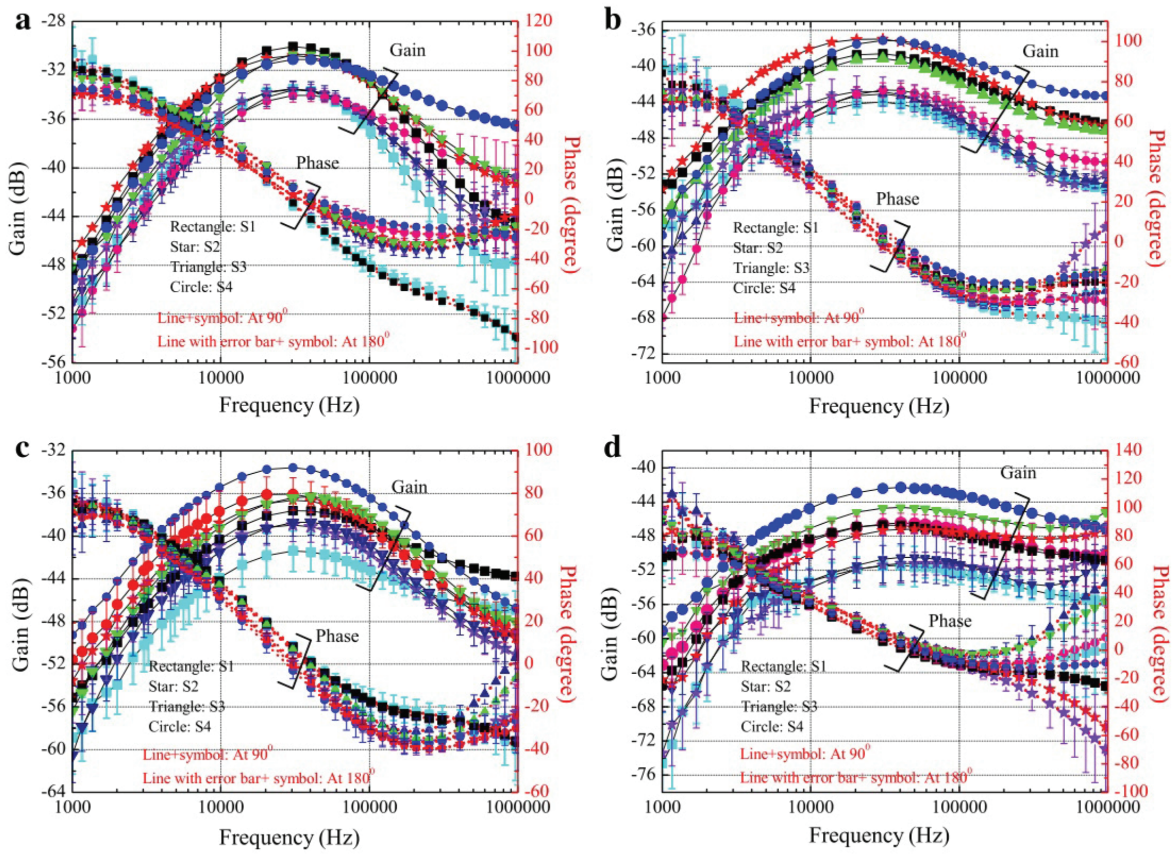

Fig. 1. Gain and phase at two joint angles for the four subjects. The values at 90° are depicted by lines with symbols. Lines with error bars (variance over 3 days measurement) and symbols represent the values at 180°. The values from channel A1A2, A1A3, B1B2 and B1B3 are displayed in sub-figure a, b, c and d, respectively. Lines with symbol rectangular, star, triangle and circle is for S1, S2, S3 and S4, respectively.

Publication(s):

[1] X.M. Chen*, S.H. Pun*, J.F. Zhao, P.U. Mak*, B.D. Liang and M.I. Vai*, "Effects of human limb gestures on galvanic coupling intra-body communication for advanced healthcare system," Biomedical engineering online, May 2016.

* Contributors with University of Macau

Sponsorship:

Macau Science and Technology Development Fund (FDCT), Research Committee of University of Macau, Shenzhen Polytechnic and Guangdong Provincial Science and Technology Plan

Channel Modeling and Power Consumption Analysis for Galvalnic Coupling Intra-body Communication

Yue Ming Gao, Yan Ting Ye, Mang I Vai, Min Du, and Sio Hang Pun

FEATURES

Low Bit Error Rate, 10^{-6}

Low power consumption, 2.3 μJ/bit

DESCRIPTION

Intra-body communication (IBC), using the human body as the channel to transmit data, has lower power consumption, less radiation, and easier linking than common wireless communication technologies such as Bluetooth, ZigBee, and ANT+ . As a result, IBC is greatly suitable for body area network (BAN) applications, such as the medical and health care field. Furthermore, IBC can be implemented in wearable devices, including smart watches, sports bracelets, somatic game devices, and multimedia devices. However, due to the limited battery capacity of sensor nodes in a BAN, especially implanted sensor nodes, it is not convenient to charge or change the batteries. Thus, the energy effectiveness of the media access control (MAC) layer strongly affects the life span of the nodes and of the entire system. Certainly, analyzing MAC layer performance in a galvanic coupling IBC is of great importance for the overall system. To obtain the attenuation properties of IBC, in vivo experiments with seven volunteers were performed.

Meanwhile, an equalizer was used to compensate the frequency distortion in consideration of frequency-selective fading characteristics of intra-body channels. In addition, a comparison of the bit error rates (BER) of different modulation methods was carried out to obtain the best modulation method. Then, the attenuation characteristics of intra-body channels were applied in a multi-node physiological signal monitor and transmission system. Finally, TDMA and CSMA/CA protocols were introduced to calculate the bit energy consumption of IBC in the practical scenario. With stable characteristics of the intra-body channels, QPSK with an equalizer had a better performance than the tests without an equalizer. As a result, the modulation method of FSK could achieve a lower BER in lower signal-to-noise ratio situations and an FSK method with TDMA for the IBC had the lowest energy consumption under different practical scenarios.

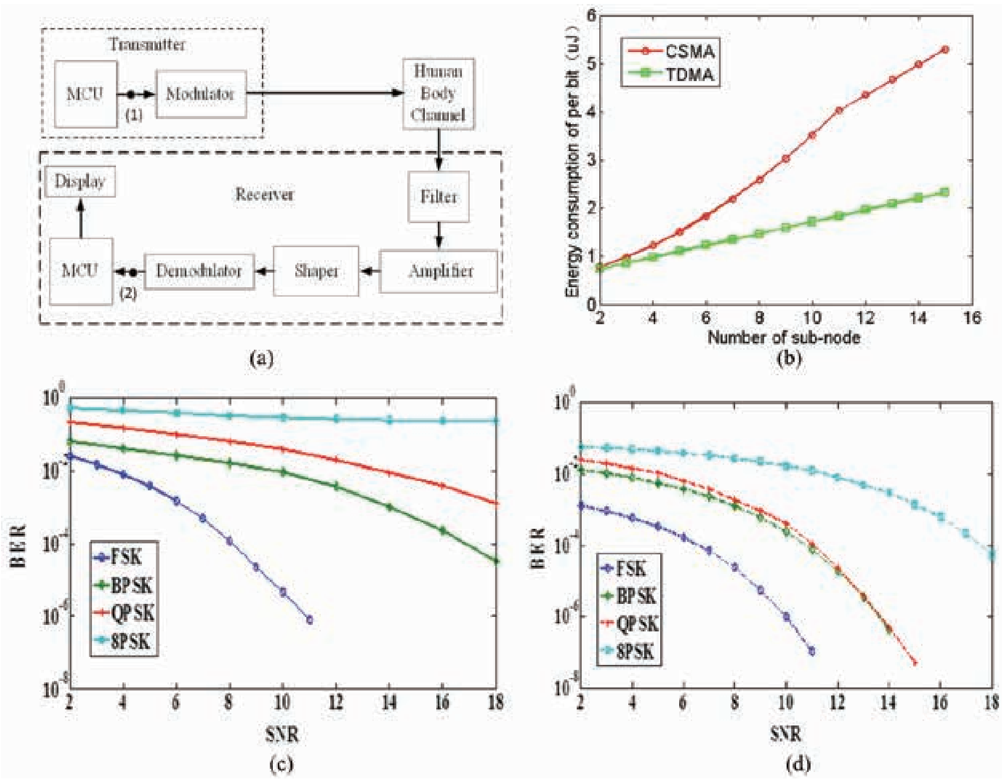

Fig. 1. (a) Diagram of intra-body communication; (b) Energy consumption comparisons of TDMA and CSMA/CA under the multi-node system; (c) BER versus SNR of four kinds of modulation method with equalizer and (d) without equalizer.

Publication(s):

[1] Y.M. Gao, Y.T. Ye, M.I Vai*, M.D. and S.H. Pun*, "Channel modeling and power consumption analysis for galvanic coupling intra-body communication," EURASIP Journal on Wireless Communications and Networking, vol. 2016, no. 106, Jun. 2016.

* Contributors with University of Macau

Sponsorship:

Chinese Ministry of Science and Technology, National Natural Science Foundation of China, Department of Education of Fujian Province and Department of Education of Fujian Province

A Novel Field-Circuit FEM Modeling and Gain Estimation for Galvanic Coupling Real IBC Measurements

Yue-Ming Gao, Zhu-Mei Wu, Sio-Hang Pun, Peng-Un Mak, Mang-I Vai, and Min Du

FEATURES

Low error, 3 dB in range of 10 kHz to 500 kHz,
9 dB in range of 500 kHz to 1 MHz

DESCRIPTION

Existing research on human channel modeling of galvanic coupling intra-body communication (IBC) is primarily focused on the human body itself. Although galvanic coupling IBC is less disturbed by external influences during signal transmission, there are inevitable factors in real measurement scenarios such as the parasitic impedance of electrodes, impedance matching of the transceiver, etc. which might lead to deviations between the human model and the in vivo measurements. This paper proposes a field-circuit finite element method (FEM) model of galvanic coupling IBC in a real measurement environment to estimate the human channel gain.

First an anisotropic concentric cylinder model of the electric field intra-body communication for human limbs was developed based on the galvanic method. Then the electric field model was combined with several impedance elements, which were equivalent in terms of parasitic impedance of the electrodes, input and output impedance of the transceiver, establishing a field-circuit FEM model. The results indicated that a circuit module equivalent to external factors can be added to the field-circuit model, which makes this model more complete, and the estimations based on the proposed field-circuit are in better agreement with the corresponding measurement results.

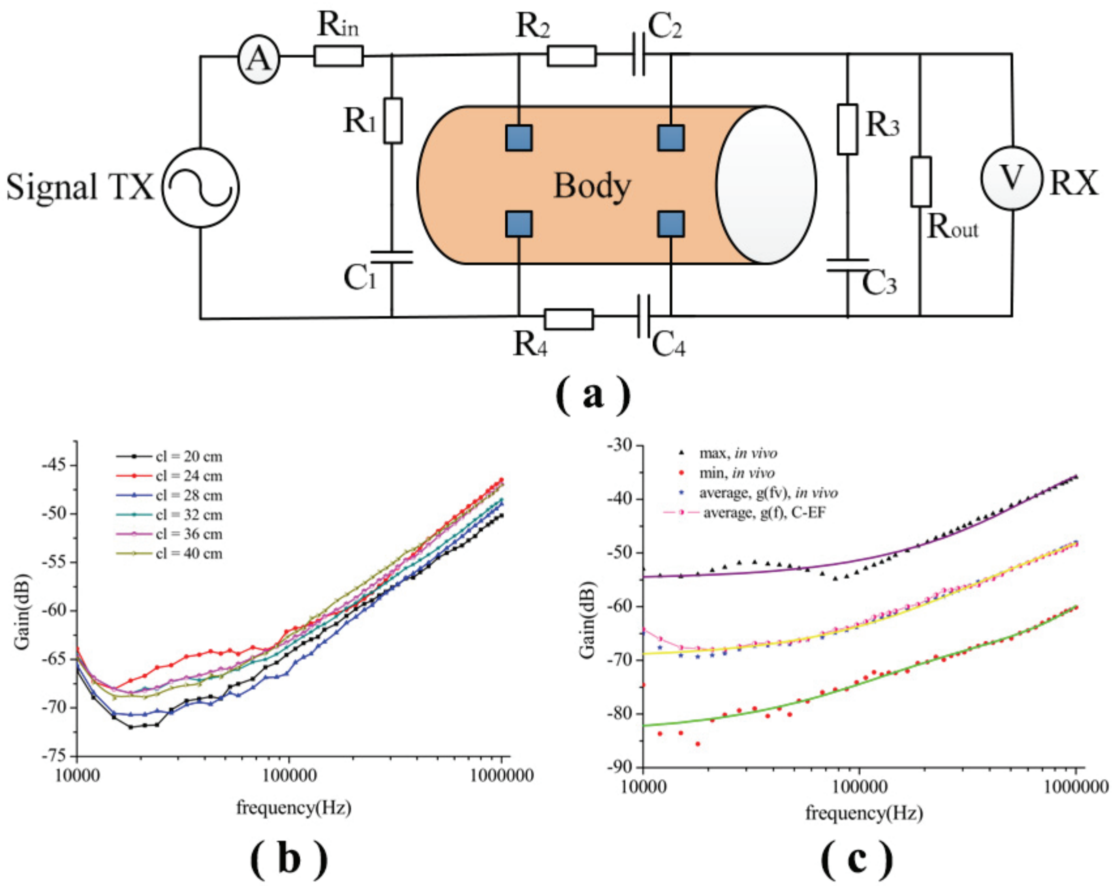

Fig. 1. (a) The field-circuit model of signal transmission path in the galvanic intra-body communication; (b) mean values of the long distance intra-body communication channel characteristic, measured on 10 subjects at different distances; (c) mean values of the long distance human body channel amplitude characteristic variation range, measured on 10 test subjects. The star curve and red dot line curve represent the average voltage gain for the channel length in the range of 20 cm.

Publication(s):

[1] Y.-M. Gao, Z.-M. Wu, S.-H. Pun*, P.-U. Mak*, M.-I Vai* and M. Du, "A Novel Field-Circuit FEM Modeling and Channel Gain Estimation for Galvanic Coupling Real IBC Measurements," Sensors, vol. 16, no. 471, 2016.

* Contributors with University of Macau

Sponsorship:

Chinese Ministry of Science and Technology, National Natural Science Foundation of China, and Department of Education of Fujian Province, China

Direct Measurement of Elbow Joint Angle Using Galvanic Coupling System

Xi Mei Chen, Shovan Barma, Sio Hang Pun, Mang I Vai, and Peng Un Mak

FEATURES

Low error, ±0.11 rad (6°)
High compatibility

DESCRIPTION

This paper proposes a simple approach to measure the elbow joint angle (EJA) using galvanic coupling system (GCS), directly; whereas, the traditional methods involved in either complex machine-learning task or arm movement models in which the consideration of model parameters are not accurate very often. First, a correlation between the EJA and GCS data has been established by defining a polynomial function based on a simple six-impedance model of human upper arm, where the EJA (θ) has been achieved by moving the forearm along the sagittal and transverse planes with different loads (empty hand, 1 and 2 kg). The coefficients of the polynomial are estimated based on the polynomial fit technique in which the actual angles (reference frame) are calculated by using motion data.

In total, eleven subjects (seven males and four females) with the age of 30 ± 6 years have been considered during the experiment. However, the GCS data of eight subjects are used to derive the correlation, exclusively. Furthermore, the influence of muscle fatigue and different loads on the derived correlation has been studied. Next, based on the derived correlation, the EJA has been measured in two parts–inside and outside tests by considering six subjects. The results show that the proposed idea can measure the EJA very effectively with error up to ±0.11 rad (6°). Moreover, in a performance comparison, the proposed approach shows its compatibility by indicating low complexity, higher accuracy, and easy to measure.

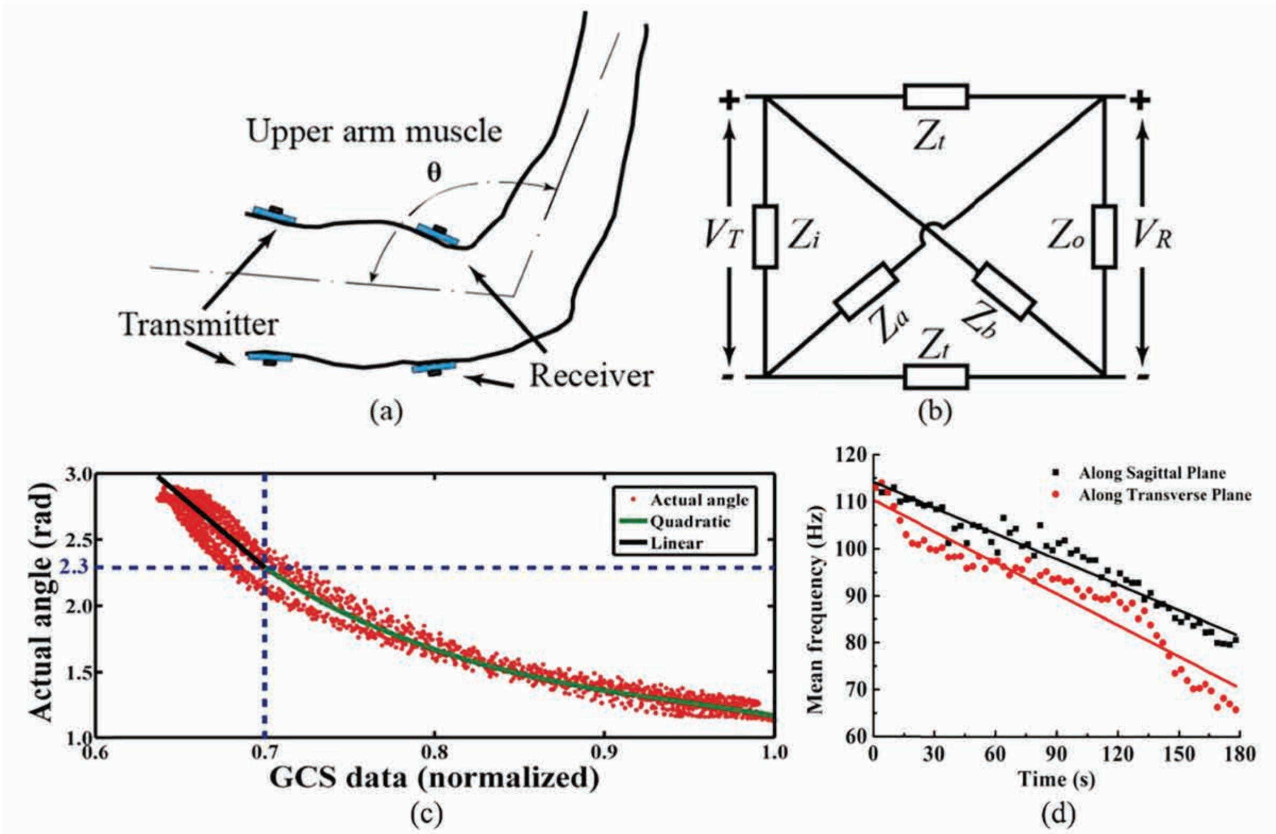

Fig. 1. (a) Schematic of the galvanic couple system on upper arm muscles; (b) Equivalent circuit model of upper arm; (c) Analysis of the curve fitting between GCS data and EJA; (d) Muscle fatigue during forearm movement (for 2 kg load).

Publication(s):

[1] X.M. Chen*, S. Barma*, S.H. Pun*, M.I Vai*, and P.U. Mak*, "Direct Measurement of Elbow Joint Angle Using Galvanic Couple System," IEEE Transactions on Instrumentation and Measurement, vol. 66, no. 4, pp. 757-766, Apr. 2016.

* Contributors with University of Macau

Sponsorship:

Macau Science and Technology Development Fund (FDCT), Research Committee of University of Macau